Design and optical characterization of an efficient polarized organic light emitting diode based on refractive index modulation in emitting layer

DUN QIAO,[1, 2] GUOJIE CHEN,[1, *] YONGKANG GONG,[3] KANG LI,[2, 6] YUANLONG FAN,[2] BO ZHANG, [2, 4] FUQIANG JIA,[5] YUSUF ABUBAKAR,[2] ADAM JONES,[2] IFIOK OTUNG,[2] AND NIGEL COPNER[2]

[1]School of Physics and Optoelectronic Engineering, Foshan University, Foshan, 528000, China
[2]Faculty of Computing, Engineering and Science, University of South Wales, Pontypridd, CF37 1DL, United Kingdom
[3]School of Physics and Astronomy, Cardiff University, Cardiff, CF24 3AA, United Kingdom
[4]Henan Academy of Special Optics Ltd., Xinxiang, 453000, China
[5]School of Electronic Science and Engineering, Xiamen University, Xiamen, 361005, China
[6]kang.li@southwales.ac.uk
*512088102@qq.com

Abstract: Luminescent liquid Crystal (LC) material is regarded as the most promising material for polarized organic light emission due to their intrinsic characteristics including orderly alignment and luminescence. Nevertheless, the optical extraction efficiency of LC based organic light emitting diodes (OLEDs) devices still requires significant effort and innovation towards real-world applications. In this paper, we propose the design of a highly linearly polarized light-emission from OLEDs with integrated refractive index nanograting in the emissive layer (EML), which is based on photo aligned luminescent liquid crystal material. The simulation results indicate that the geometrically optimized polarized device yields an external quantum efficiency (EQE) up to 47% with a polarized ratio up to 28 dB at 550 nm emission wavelength. This conceptual design offers a new opportunity to achieve efficient polarized organic luminescence, and is, to the best of our knowledge, the first approach that enhances the light extraction of OLEDs based on luminescent liquid crystal via index grating in the EML.

1. Introduction

Organic light emitting diodes (OLEDs), which were invented 1987 [1], have been significantly developed in the last three decades. Nowadays, OLEDs are successfully applied in both portable electronic devices and televisions. With the development of photo luminescent material, the internal quantum efficiency of OLEDs has been improved to nearly 100% utilizing phosphorescent material [2]. However, the optical out-coupling efficiency still places a considerable limitation on the overall efficiency of OLEDs. Due to the optical loss caused by the mismatch of refractive index between each layer and surface plasmon polariton (SPP) on the metal-organic interface, only 20% of energy can be ultimately outcoupled. Several approaches have been proposed to eliminate these optical losses. In general, scattering structure is one of the main methods to enhance the optical extraction of OLEDs. T. Yamasaki proposed the first scattering structure to increase the efficiency of OLEDs in 2000 [3]. Since then, various structures to eliminate different losses have been proposed. The micro-lens array [4-8] and scattering layer [9-11] have been adopted as external structures to decrease the substrate loss on the interface between substrate and electrode. Periodic structures including diffraction grating [12, 13], corrugated structure [14, 15], low-index grids [16-18] and Bragg grating attached on the electrode [19] have been utilized to recover the losses inside the multi-layer structure of OLEDs.

Most research on OLEDs has focused on unpolarized emission. The polarized OLEDs are the prominent next generation light source of liquid crystal displays (LCDs) backlight and three-dimensional display systems. Since Dyreklev et al. first reported directly producing linear polarized emissions by using aligned polymer film in 1995 [20], alignment of the emissive layer based on luminescent liquid crystal material in OLEDs has become a key method for achieving highly polarized emission and has attracted a lot of interest. Various approaches have been developed to produce an aligned emitting layer, such as an electrostatic field generated by mechanical friction [20, 21], Langmunir-Blodgett (LB) deposition technique [22] and application of self-organization properties of liquid crystal material [23]. The aligned emitting layer is typically composited by rod-like uniaxial molecules- such as oligofluorene, thiophene and oxadiazole derivatives. For most of the rod-like molecules, their transition dipole moments are along their long axis [24], thus, high effective polarized emission can be achieved by orderly orienting these molecules.

Although incorporating aligned material in the emitting layer does implement polarized emission, the anisotropy of the optical constants of emitting layer is correspondingly changed due to its high relevance to the orientation of molecules [24]. More specifically, the in-plane ordinary refractive index is raised, which increases the optical loss due to transverse electric (TE) mode and further influence the optical extraction efficiency of the whole device. However, the molecule orientation dependent anisotropy makes it feasible to manipulate the refractive index of emitting layer, thereby enhancing the extraction efficiency. Previous work has reported outcoupling characteristic modifying of OLEDs by modulating refractive index to form refractive index pattern [25]. Logically, the precise alignment methods and appropriate optical structure design are the two main challenges for achieving high efficiency polarized OLEDs.

In this paper, we propose a simulation based design of enhanced light extraction polarized OLEDs devices with a periodic index difference nano structure based on refractive index manipulation, which is feasible by utilizing photoalignment luminescent liquid crystal (LC) [26]. The photoalignment luminescent LC is achieved by compounding photoalignment moiety at both ends of the chain of the emissive small-molecules with rod-like shape, the photoalignment moiety will crosslink to each other under ultraviolet (UV) exposure, which forces the long axis of the molecules to align uniformly. Therefore, periodic refractive index changed nano-pattern can be precisely produced and controlled by exposing the material under a UV interference pattern [26]. By introducing the refractive index grating, the EQE of the devices is enhanced up to 56% with preferable geometric parameters at 550 nm emission wavelength. Furthermore, a structure design with an extra uniformly aligned layer is proposed and researched to improve the polarized ratio to 28 dB under the premise that the EQE has been enhanced via refractive index grating. Detailed analysis indicates that both TE and transverse magnetic (TM) mode losses are recovered and outcoupled via the refractive index grating while the grating modulates the polarization characteristic as well. The EQE spectrum in the visible band of 400 to 700 nm is investigated. The key results are compared at the wavelength of 550 nm which is chosen to close to the sensible wavelength for photopic vision (peak at 555 nm).

2. Optical losses analysis of polarized OLEDs based on luminescent Liquid Crystal

The orientation of the molecules inside the emission layer deeply influences both the refractive index and emitting polarizability. For a rod-like molecule shown in Fig. 1, the transition dipole moment generally coincides with its long molecule axis [24], and the orientation of the molecule dominates the direction of electric field vector during emission. If all the molecules in the EML can be perfectly aligned in horizontal direction, linearly polarized emission can be achieved. However, the alignment leads to anisotropy in the optical constant. In the case of molecules with rod-like shape, molecular polarizability along the long axis is significantly larger than the other directions. This is because electrons move inside an organic molecule more easily than between the molecules, which results in the anisotropy in molecular polarizability

[21]. Therefore, a high birefringence can be achieved in a horizontally aligned EML. In this homogeneous aligned EML, the refractive index component in the y axis, n_y, is significantly enhanced because the long molecular axes are totally oriented in the y direction, as a result, the optical loss of the TE mode is increased.

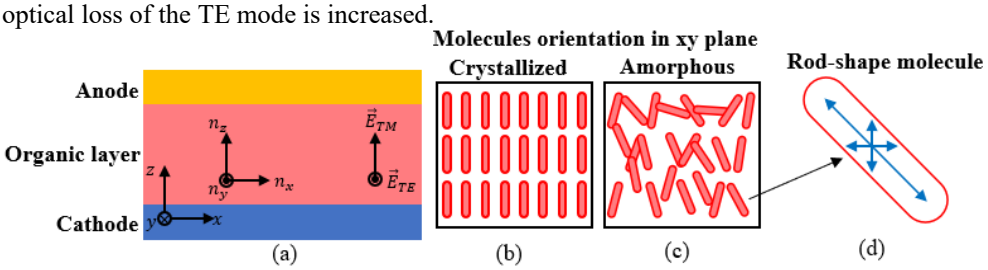

Fig. 1. (a) Typical 2D structure of OLEDs. Top view of the EML with (b) aligned rod-like shape molecules and (c) random distributed rod-like shape molecules. (d) Transition dipole moment of rod-like shape molecule.

Figure 2(a) and (b) illustrate the simulation model of OLEDs with amorphous and crystallized EML, respectively. From the top to the bottom of the structure, a 100 nm ITO layer represents the anode, 60 nm α-NPD is adopted as hole transport layer (HTL), 100 nm LC material layer is EML, 60 nm Alq3 is electron transport layer (ETL), and 300 nm Aluminum is the reflective cathode for the devices. The EML material we adopted is luminescent LC based on BDAVBi derivation. Yokoyoma et al. had investigated the anisotropy refractive index of BDAVBi film with molecules oriented in plane but without alignment [27, 28], in other words, amorphous in plane. The largest value they tested are n_o ≈2.4 and n_e ≈1.8, respectively. The refractive index of isotropic BDAVBi film can be calculated with following equation [29]:

$$n_{iso} = \sqrt{\frac{2{n_e}^2 + {n_o}^2}{3}} \tag{1}$$

where n_e and n_o are the extraordinary (vertical) and ordinary (horizontal) refractive index, respectively. Because the long molecular axes in our homogeneous aligned LC material are oriented along the y axis ideally, it is assessed that the n_y for our homogeneous aligned LC is not less than n_o Yokoyoma tested. Therefore, we adopt n_y≈2.4, $n_x = n_z$≈1.8, n_{iso}≈2.1 as reference refractive index. Callens et al. has also investigated the effect of anisotropic ETL and HTL on the outcoupling efficiency [30]. The refractive index and thickness of each layer used in the simulation are shown in Table 1.

Table 1. Refractive indices and the thickness of each layers

layers	Material	Thickness	refractive index
substrate	Glass	3000 nm	1.5
anode	ITO	100 nm	1.8
HTL	α-NPD	60 nm	1.78
EML	LC Material (BDAVBi derivation)	50~150 nm	n_y≈2.4, $n_x = n_z$≈1.8, n_{iso} ≈2.1
ETL	Alq_3	60 nm	1.76
Cathode	Aluminum	300 nm	1+6j

In general, OLEDs with a multi-layer structure forms an optical cavity, and the spatial distribution of different optical eigenmodes determines the optical losses of OLEDs and provides a basis for the design of a nano structure to enhance optical extraction. Therefore, by utilizing finite difference eigenmode (FDE) solver in Lumerical FDTD software, we perform eigenmode analysis for structures based on the parameters in Table 1 to identify the optical losses in polarized OLEDs with crystallized EML. As shown in Fig. 2(c), for the model with

amorphous emitting layer, the loss channel of TE eigenmode is mainly located at the interface between ITO anode and HTL, which behave like typical conventional OLEDs structures [31]. However, in Fig. 2(d) for the crystallized model, due to its higher in-plane refractive index n_y, the TE mode loss channel moves inside the emitting layer. Therefore, unlike most of the previous research that focused on the design of the optical structure located at the anode and cathode interfaces of conventional OLEDs to improve the extraction efficiency, the work in this paper focuses on enhancing the extraction efficiency and EQE via periodic index change grating in the EML.

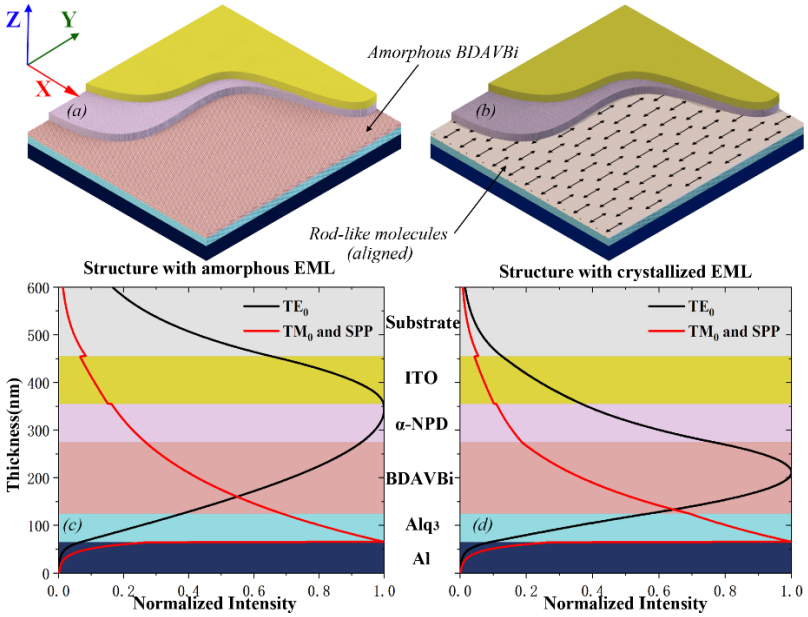

Fig. 2. (a) Multi-layer structure of OLEDs with amorphous emitting layer. (b) Structure of OLEDs with crystallized emitting layer. (c) Normalized intensity distribution of lossy mode in OLEDs with amorphous emitting layer. (d) Normalized intensity distribution of lossy mode in OLEDs with crystallized emitting layer, the TE lossy mode is confined in emitting layer due to high ordinary refractive index.

3. Light extraction by refractive index gratings in EML

According to the above results and discussion, the crystallization of the emitting layer indeed impacts the EQE of devices, where anisotropy of aligned EML leads to a significant TE waveguide mode loss channel at the EML. To suppress this energy loss and recover it to the output, we propose a refractive index grating in the EML as shown in Fig. 3. This grating expands along the x axis and can be potentially fabricated based on the photo-crosslink properties of the emitting material [26]. By compounding photo alignment moiety to BDAVBi molecules, the formed BDAVBi derivation can exhibit liquid crystal characteristics. When the LC material is exposed to the interference fringes formed by UV light, the material in the exposed area (bright fringe area in Fig. 3) undergoes photochemical cross-linking and curing to stably keep the rod-like molecules arranged in order, i.e., in one direction. After that, the entire structure is heated so that the area where the photochemical cross-linking does not occur becomes a liquid with a disorderly distribution of rod-shaped molecules due to the increase in temperature. This is followed by UV exposure on all areas. The amorphous regions are also crosslinked and cured. Finally, a stable index change grating structure is formed, which consists of highly stable crystallized area and amorphous area alternating as shown in Fig. 3.

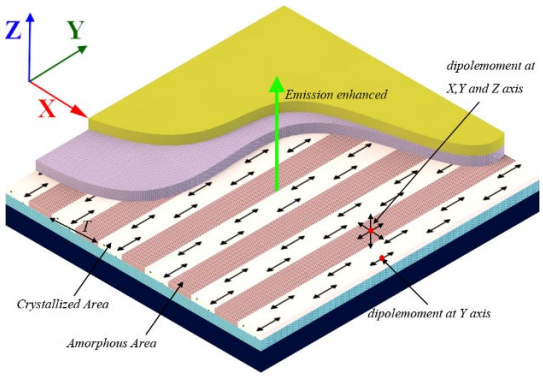

Fig. 3. The OLEDs structure with refractive index grating in its emitting layer. The amorphous and crystallized areas are arranged along the *x* axis; T is the period of grating; and F=Λ/T represents the fill factor of grating, and Λ is the width of crystallized areas.

We perform the Finite-Difference Time-Domain (FDTD) method for the grating model based on Lumerical FDTD solution software. The structure of the grating model is shown in Fig. 3. The material and thickness of each layer used in this model is generally the same as shown in Table 1. The main difference here is that the refractive index gratings formed by periodical isotropic and anisotropic area in the EML is considered in this model. As a comparison, an EML with crystallized area without formed gratings is also simulated as a reference to study the enhancement in outcoupling efficiency and EQE. The reference devices in the remainder of the text will have the same geometric parameters as the grating devices.

Our simulation is based on the classic 2-dimension dipole model on *xz*-plane, while a dipole array located in the center of z span of the EML represents the excitons [32]. For amorphous EML, the excitons inside it have random oscillation directions. To perform it precisely, each dipole in the amorphous area has three representative oscillating directions perpendicular to each other, which are in plane direction (*x* and *y* axis) and vertical direction (*z* axis). In contrast, in the crystallized area has the long axis of rod-like molecules is all aligned along the *y* axis as shown in Fig. 3. Their transition dipole moments and the oscillating direction are set along the *y* axis. Additionally, to simplify the simulation, it is assumed that the amorphous and crystallized areas have the same molecular density and conductivity, which ensures that the dipole amount in the two areas are equal.

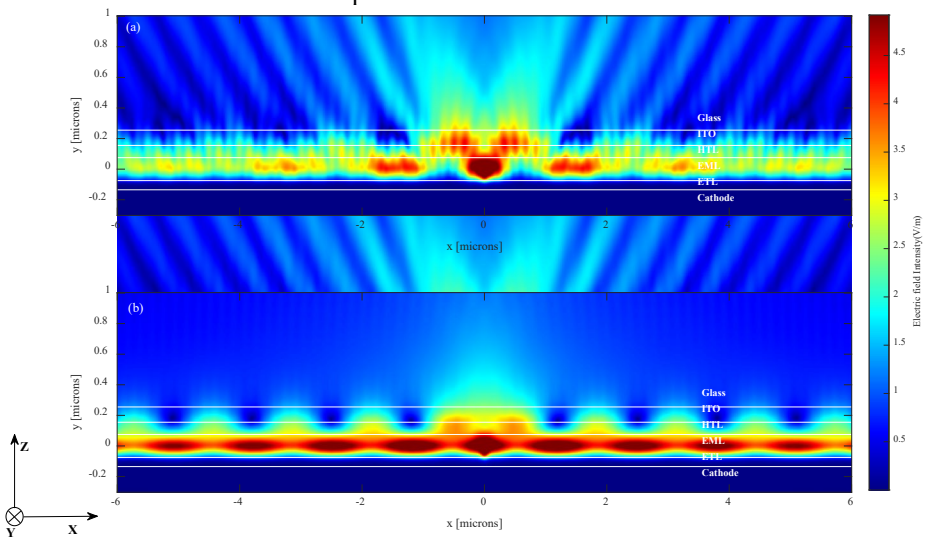

Fig 4. Simulated electric field intensity distribution via side view for (a) grating structure, and (b) non-grating structure.

We implement a simple 2-dimension one dipole model simulation to verify the optical extraction effect of the refractive index change grating. The oscillation direction of the dipole is set along the *y* direction. Figure 4 shows the simulated electric field intensity from section view of both grating and non-grating structure at 550 nm emission wavelength.

Figure 4(b) reveals clear periodical intensity patterns in the EML layer along the *x* axis, which are the TE waveguide modes transmitting in the EML layer. Since the dipole moment is set at the *y* axis, its waveguide modes perform alternating strong and weak patterns along the *x* axis. Besides, the intensity of the waveguide modes are decreasing along the x axis due to the absorption of the medium. In contrast, the TE waveguide modes experience dramatic decrease along the *x* axis in the EML with the grating structure as shown in Fig. 4(a). Additionally, a series of alternating fringes are observed in the glass layer of the OLED with a grating structure. The waveguide modes in the EML are extracted, and light outcoupled in the glass substrate is enhanced.

The EQE is commonly adopted to present the performance of OLEDs devices, the EQE of OLEDs is normally derived by following equations.

$$EQE = \eta_{out} \times IQE \tag{2}$$

$$IQE = \frac{\gamma_{rad}}{\gamma_{rad} + \gamma_{nrad}} \tag{3}$$

Here, η_{out} is the optical outcoupling efficiency of the structure, and IQE is the internal quantum efficiency of the EML material. In our model, the IQE is considered as 0.8 to simplify the simulation because the BDAVBi is a kind of fluorescent material. The γ_{rad}=0.8 and γ_{nrad}=0.2 are, respectively, the radiative and nonradiative decay rates of the EML. However, the energy of the dipole in homogeneous media is different from that in free space, the emission rate of the dipole is deeply influenced by the surrounding media and structures. Hyunsu Cho et. al. investigated the influence of the Purcell factor of the dipole system to the simulation accuracy, and proposed the following modified equation for the EQE [33]:

$$EQE_{full} = \gamma_{rad} \times \eta_{out} \times \frac{1}{1 - \gamma_{rad} + P(\lambda)\gamma_{rad}} \tag{4}$$

Here, $P(\lambda)$ is the Purcell factor of the model, which is the ratio of dipole power to the source power in FDTD solver. Note that η_{out} can be obtained in simulation by normalizing the outcoupled power to the source power, and the outcoupled power is the total power received by a one meter radius semi-circle at far-field. Therefore, EQE can be calculated using the above equation.

Polarization performance is usually the main target for the design of these devices. The polarized ratio is generally applied for estimating the performance of polarized OLEDs and can be calculated based on the following equation [34]:

$$polarized\ ratio = 10 \cdot log\left[\frac{T_{TE}}{T_{TM}}\right] \tag{5}$$

where T_{TM} and T_{TE} are the transmission of TM and TE polarized light, respectively, this transmission being the ratio of outcoupled power to original dipole power.

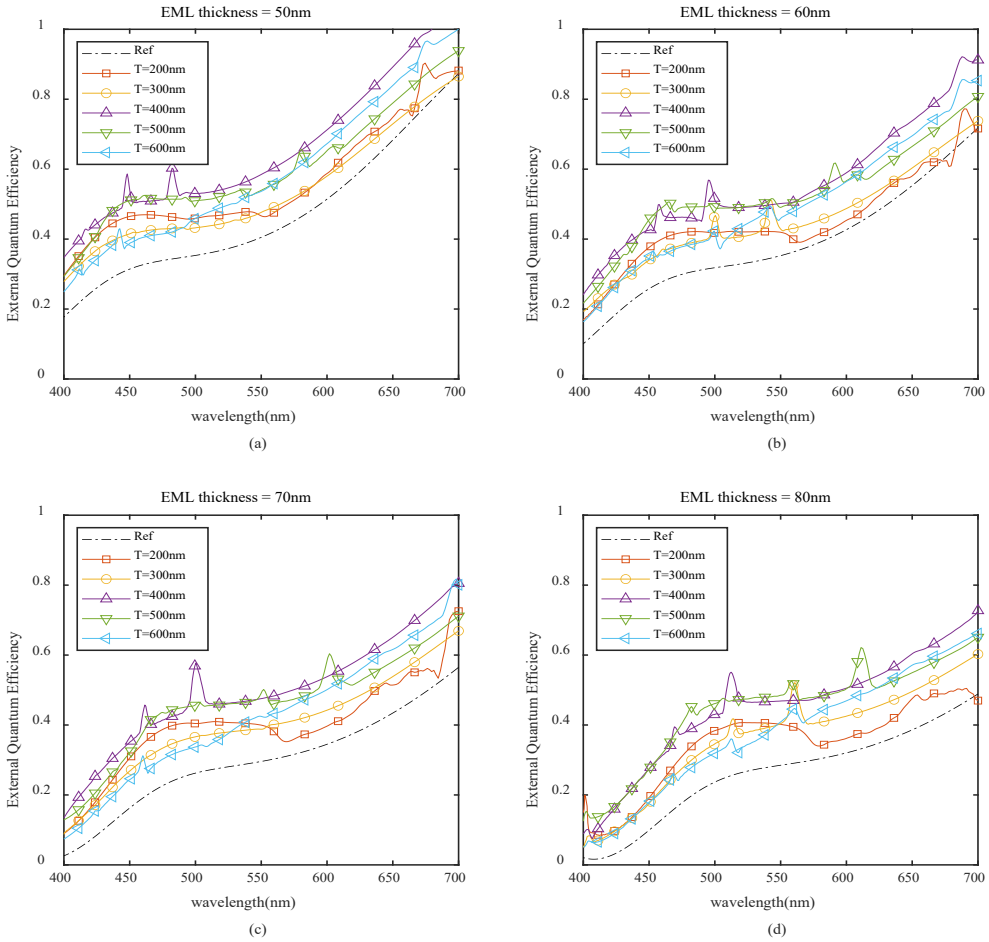

Fig. 5. EQE spectrum simulated for the reference device and devices with grating structure with different period and different thickness of EML. (a) The EQE of grating period from 200 nm to 600 nm with EML thickness at 50 nm. (b) The EQE of grating period from 200 nm to 600 nm with EML thickness at 60 nm. (c) The EQE of grating period from 200 nm to 600 nm with EML thickness at 70 nm. (d) The EQE of grating period from 200 nm to 600 nm with EML thickness at 80 nm.

Figure 5 shows the simulation results of EQE for grating structures with periods from 200 nm to 600 nm and EML thickness from 50 to 80 nm. The reference (dotted) curve in each subplot (a) to (d) of Fig. 5 represents the EQE of a structure with total anisotropic EML at each thickness. Generally, these four groups of curves show a trend of red shift when the thickness of the EML layer increases. For each subplot, the EQE of structures with grating periods from 200 nm to 600 nm all show enhancement, which indicates that the refractive index grating can enhance the EQE of whole devices. With the increase of grating period, the EQE in all four figures experience an initial increase and then a drop after the periods exceed 400 nm, this is because the grating structure with 400 nm period reaches lower Purcell factor compared with other periods, which is determined by the medium and cavity surrounding the dipole emitter. According to Eq. (4), higher EQE can be achieved at lower Purcell factor. At the wavelength of 550 nm, the structure with a grating period of 400 nm and EML thickness of 50 nm shows the highest EQE.

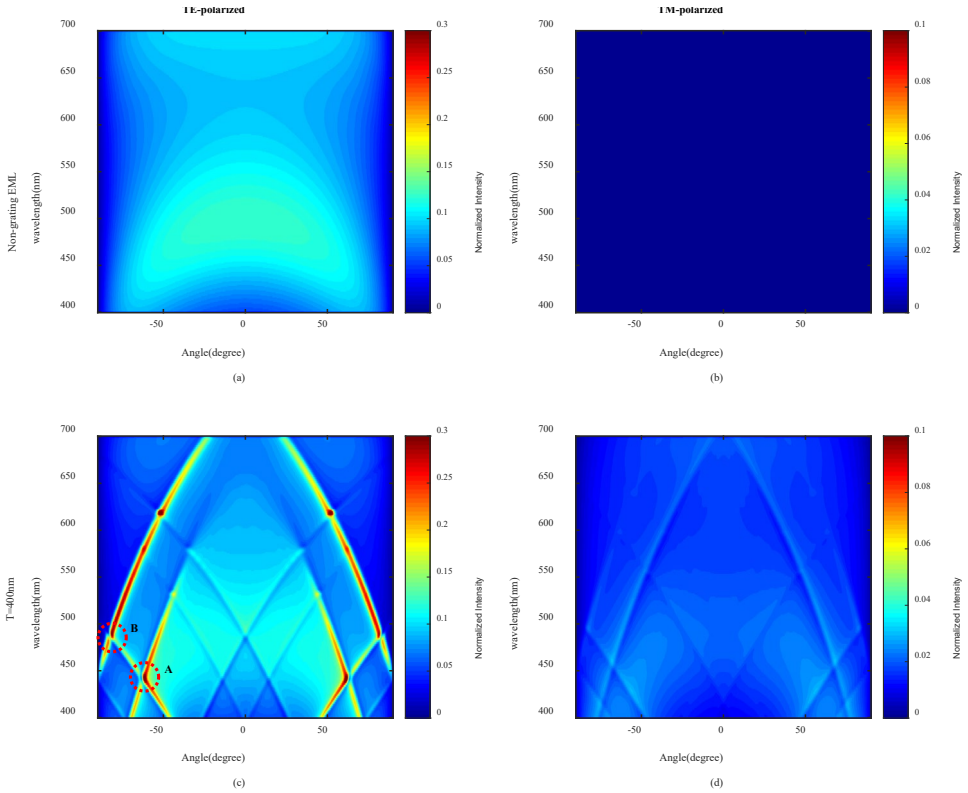

Fig. 6. Simulation of the far field electric intensity distribution of reference devices (a, b) and grating structures (c, d) in TE and TM polarization, respectively (T=400 nm, and EML thickness is 50 nm).

It is noticeable that some EQE spectrum in Fig. 5 has several peaks, which are caused by the overlap between different dispersion orders of optical modes [35]. Figure 6 shows the electric intensity distribution in the far-field for structures with a grating period of 400 nm and for non-grating structures. The EML thickness is 50 nm in both cases. The far-field profiles are simulated with respect to changes in both emission angle and wavelength. EQE spectrum of 400 nm grating period has obvious peaks around the wavelengths of 450 nm and 480 nm in Fig. 5(a). Correspondingly, its far-field distribution in Fig. 6(c) shows the overlapping points of TE dispersion at wavelengths of 450 and 480 nm, which are point A and B, respectively. Every peak of the EQE curves in Fig. 5(a) has a corresponding overlapping point in its far-field distribution. Generally, the effectiveness of refractive index gratings leads to the overall lifting of EQE curves evident in Fig. 5(a), which manifests as a brighter area in Fig. 6(c, d) compared with the reference non-grating device shown in Fig. 6(a, b). In addition, Fig. 6(b) does not exhibit any pattern, because the EML of non-grating model is totally crystallized, which means that all the dipoles in this model oscillate in the same direction and emit in the same polarization, so no power of TM mode can be observed in the far-field of the non-grating model. In summary, the peaks, or overlapping points indicate specific enhancement at corresponding wavelength. With these characteristics, grating structures enhance the optical extraction and EQE of entire devices. As the grating is designed to expand in plane, TE mode experiences higher intensity at overlapping points than TM mode, which meets the purpose of our design.

Although the EQE of each period and thickness of grating shows obvious enhancement, the polarization performance of all the grating structures is not ideal. Figure 7 shows that the polarized ratio of structures with different grating periods and thickness are generally lower than 10 dB. To further improve the polarized performance, an investigation of the effects of fill factor on polarized ratio is required, and the optimal period of the structure must first be determined. It is obvious that a grating with 500 nm period shows the highest polarized ratio in

all thicknesses, and EQE of 500 nm period grating structure with 50 nm thickness is acceptable. Consequently, the structure with 500 nm period and 50 nm EML thickness, which shows 51.5% EQE (see Fig. 5(a)) and 8 dB polarized ratio (see Fig. 7(a)) at 550 nm emission wavelength, is chosen as the ideal model for further optimization of polarized performance.

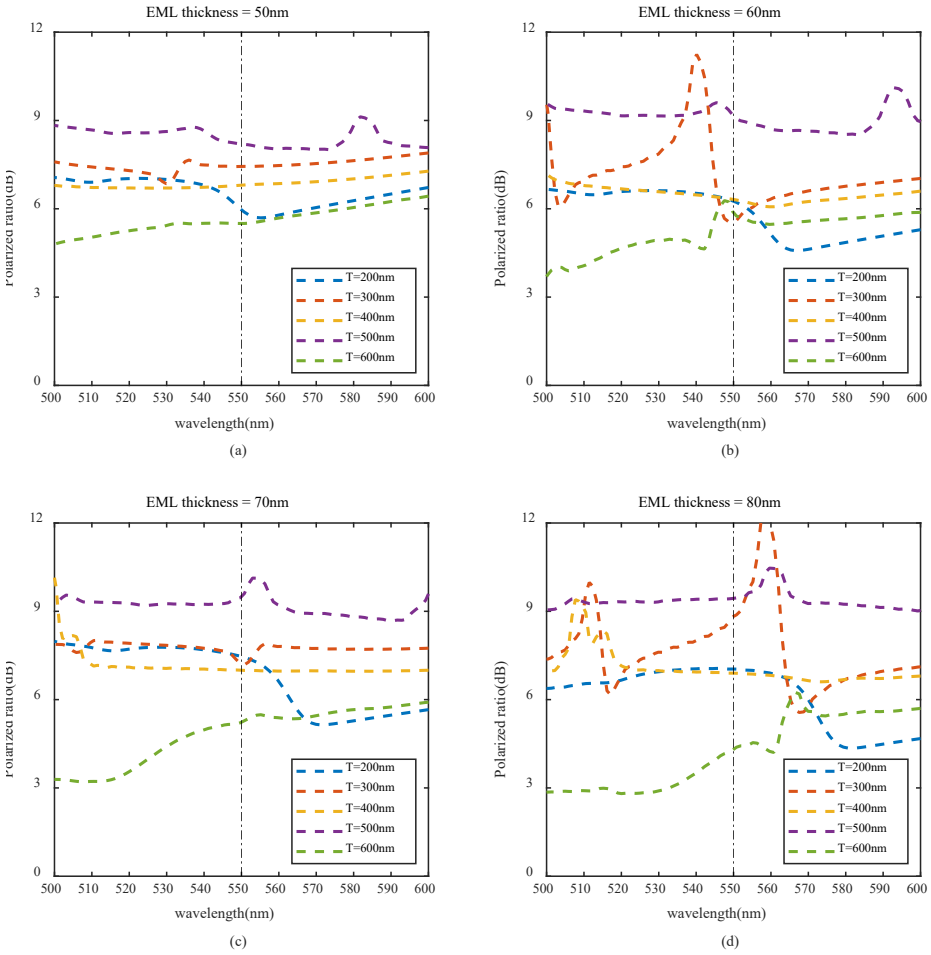

Fig. 7. Polarized ratio simulated for the reference device and devices with grating structure with different period and different thickness of EML. (a) The polarized ratio of grating period from 200 nm to 600 nm with EML thickness at 50 nm. (b) The polarized ratio of grating period from 200 nm to 600 nm with EML thickness at 60 nm. (c) The polarized ratio of grating period from 200 nm to 600 nm with EML thickness at 70 nm. (d) The polarized ratio of grating period from 200 nm to 600 nm with EML thickness at 80 nm.

To enhance the polarized ratio, we first investigate the influence of the fill factor on the polarized ratio. The fill factor of a grating is the ratio between the width (Λ) of a crystallized area and the grating period (T). Unlike in the previous simulation, the amounts of dipoles in both crystallized area and amorphous area are proportionally adjusted with the corresponding fill factor. A series of simulation with fill factor from 0.3 to 0.7 at period T=500 nm is applied. As shown in Fig. 8(b), the polarized ratio drops slightly with an increase in fill factor. Besides, the increase of the crystallized area leads to an increase in the effective refractive index of the EML layer, which further influences the EQE performance. In Fig. 8(a), EQE experiences a decrease as the fill factor increases from 0.3 to 0.7. In conclusion, the increase of the fill factor merely impacts polarized ratio for about 1.0 dB however leads to a decrease of EQE for 10%. Thus, an alternative method to enhance the polarized ratio is required.

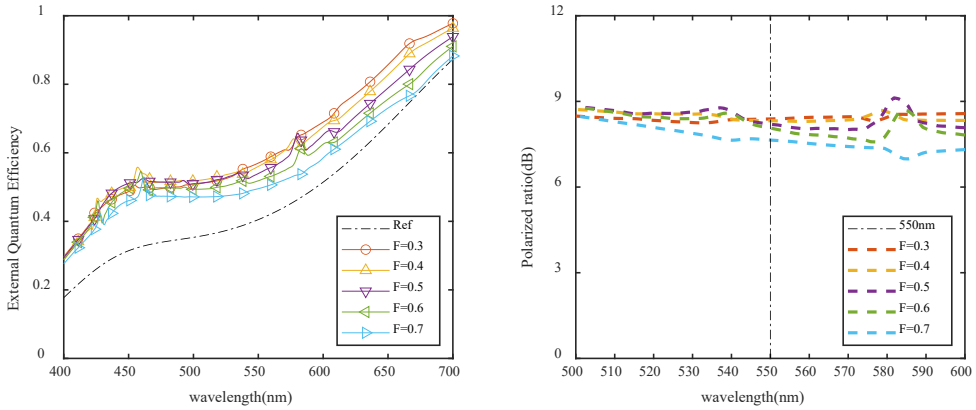

Fig. 8. (a) EQE simulated for the reference device and devices with grating structure with different fill factor. (b) The polarized ratio of grating structure with different fill factor F=Λ/T (T=500 nm).

4. Enhancing polarized ratio with extra crystallized emitting layer

In section 3, the EQE and polarized ratio of OLEDs with grating structure employing LC material as EML material is discussed, showing significant EQE enhancement achieved by inducing index change grating. However, the polarized ratio remains low and at a level below 11 dB. To improve the polarized performance without hindering EQE enhancement caused by gratings, an extra crystallized emitting layer is introduced based on the previous design. The simulation model is shown in Fig. 9. An additional layer of crystallized EML is inserted beneath EML with designed grating structure. Based on the optimized design parameter of grating obtained in Section 3 (T=500 nm, F=0.3, and EML thickness with 50 nm), simulations are implemented to investigate the influence of extra layer thickness d on EQE and polarized ratio.

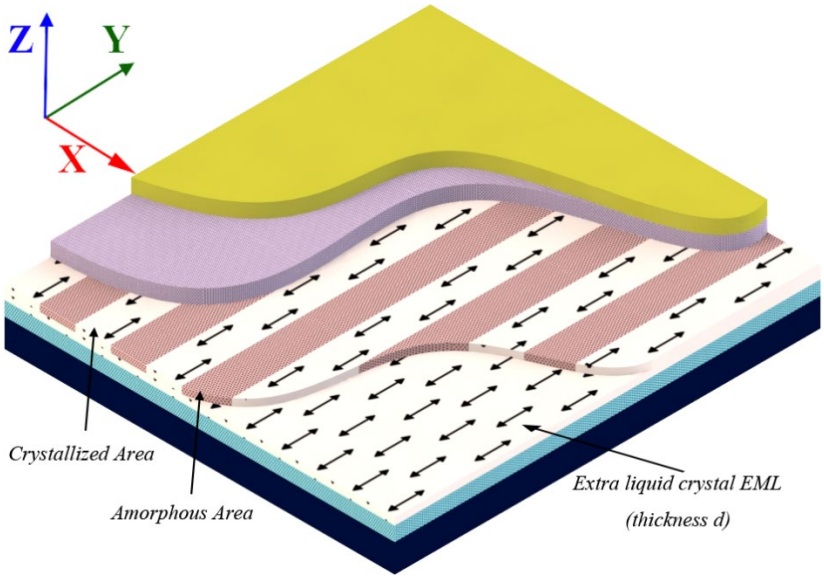

Fig. 9. The OLEDs structure with an extra crystallized emitting layer of thickness d underneath the grating structure.

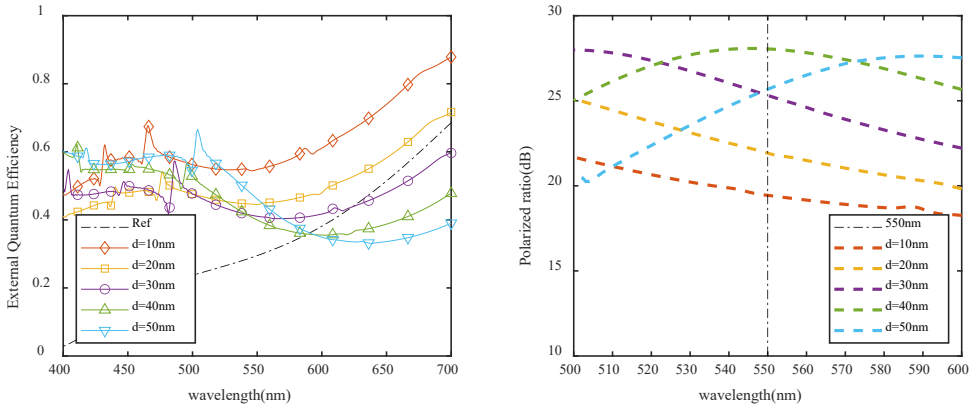

Fig. 10 (a) EQE spectrum of the reference device and devices with grating structure having various thicknesses d of an extra emitting layer. (b) The polarized ratio of a structure with various thicknesses d of an extra emitting layer (T=500 nm, and F=0.3).

Figure 10 illustrates the EQE and polarized ratio with change of thickness of extra layer d. The reference (dotted) curve in Fig. 10(a) is the EQE from the model employing a totally crystallized EML with 60 nm thickness, which is the sum of the thickness of the grating layer (50 nm) and the thickness (10 nm) of the extra layer. It is remarkable that, in the wavelength of 500 to 700 nm band, the EQE spectrum in Fig. 10(a) exhibits a decrease as d increases. This is because the increasing thickness leads to larger optical thickness between the cathode and anode, which moves the outcoupling center of the cavity and further influences the EQE in the desired wavelengths. Because the polarized ratio is significantly enhanced, this decrease in EQE is acceptable. As expected, the polarized ratio is improved up to 28 dB at the wavelength of 550 nm when d increases to 50 nm as shown in Fig. 10(b). This result compares favorably with the literature [36], where the highest polarized ratio of OLEDs based on luminescent liquid crystal material is reported to be around 20.3 dB. Furthermore, based on our simulations with different geometrical dimensions of the structure, it is noticeable that the enhanced waveband is totally adjustable by changing the thickness of the extra layer and the whole EML layer, and at the same time, the polarization ratio can also be guaranteed to be at a higher level.

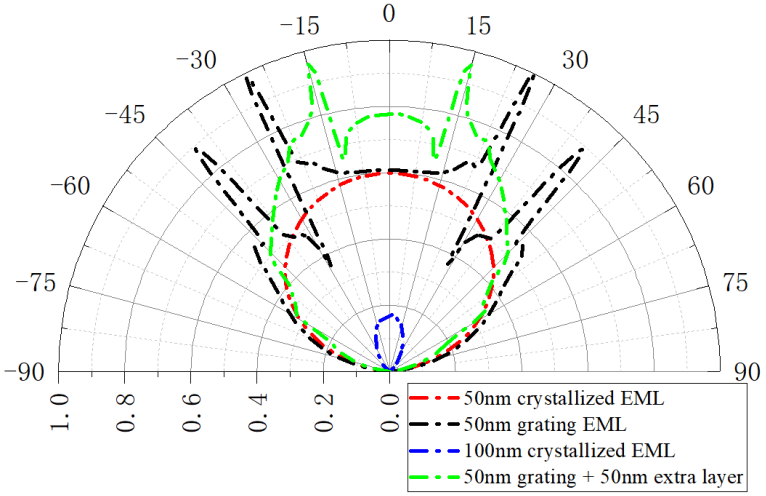

Fig. 11. Normalized far-field intensity as a function of the viewing angle (T=500 nm, F=0.3, and emission wavelength is 550 nm).

The far-field angular profile of emission is another important value to estimate the angular visibility of OLEDs devices. In Fig. 11, the red and blue curves are structures with a total

crystallized EML (without grating) of 50 nm and 100 nm thickness, respectively. It is remarkable that the intensity of 50 nm thickness is much higher than the 100 nm thickness, this is because of the red shift trend due to increasing thickness. A minimum point of the curve moves closer to the 550 nm emission wavelength with the thickness increasing from 50 nm to 80 nm (see Fig. 5). This trend is continuous with the further thickness increasing. The green curve in Fig. 11 shows that the emission intensity of the structure with d=50 nm extra crystallized emitting layer is enhanced in full range of emitting angle. Comparing with the structure with only 50 nm grating EML (black curve), the 50 nm grating plus 50 nm crystallized layer (without grating) structure has better uniformity in the full viewing range, and its curve is similar to a Lambertian radiator, which is better for application in display.

5. Future work

In brief, by adjusting the optical cavity thickness and grating period, an optimized structure is discovered for polarized OLEDs based on LC material formed by BDAVBi derivation. By compounding photo alignment moiety to the end of BDAVBi chain, this structure design is promising and feasible under UV exposure. The simulation results indicate that the efficient OLED emission with high polarized ratio can be achieved. However, the perfect alignment of molecules is not realistic, and the degree of molecules orientation could impact the polarized ratio of real devices. This is essential to be addressed in the next stage of study. Furthermore, we are pursuing the next stage of this project to co-operate with our industrial partners to synthesize the derivation with rod-like molecules. By replacing the BDAVBi luminescent core with other organic luminescent material having rod-like shape molecules [26, 30] and adopting the optical design introduced in this paper, enhanced polarized OLEDs in other color including red and green can possibly be implemented. In addition, the polarized ratio could be further improved by eliminating the emission from the amorphous area, which is usually achieved by doping to decrease the conductivity of the amorphous area [37]. We are seeking co-operation with our partners to synthesize the different materials for the next step of this experimental study.

6. Conclusion

A conceptual design of a high linearly polarized OLEDs with a refractive index grating in the emitting layer has been proposed and researched via numerical simulation. The influences on EQE and polarized ratio induced by EML thickness, grating period, grating fill factor and extra layer thickness are investigated comprehensively. A change of EML thickness can move the center of the emission waveband of the entire structure, and a change of grating period influences the enhancement of EQE. The grating fill factor only slightly influences both the EQE and polarized ratio. Furthermore, an extra crystalized emission layer significantly improves the polarized ratio with good EQE in the designed wavelength band. Finally, the optimized structure with grating period of 500 nm and filling factor of 0.3 for emitting layer and extra emitting layer with thickness of 50 nm shows 47% EQE and up to 28 dB polarized ratio at 550 nm emission wavelength. 56% EQE and 19 dB polarized ratio are achieved as well at 550 nm emission wavelength with the flexible designed structure (T=500 nm, F=0.3, and d=10 nm). In addition, the optimized structure has significant light extraction enhancement at each viewing angle. Due to the nature of the photo-alignment and photo-crosslink of LC material based on BDAVBi derivations, this grating structure is easy to fabricate, and therefore could be a promising approach for the polarized OLEDs light source with scaling to high-volume manufacturing.

Funding

Guangdong-Hong Kong-Macao Intelligent Micro-Nano Optoelectronic Technology Joint Laboratory (Project No. 2020B1212030010); Joint PhD Program between Foshan University (China) and University of South Wales (United Kingdom); Henan International Joint Laboratory of Special Light Source.

Acknowledgments

The authors thank Jiuyuan Zhu, Yang Zhou, Angharad Curtis, Chris Price, Dr. Peter Rees, Dr. Hatef Dinparasti Saleh, Prof. Antony Davies, Prof. Qiuyu Nie, Prof. Jin Wen and Prof. Yani Zhang for useful discussions.

Disclosures

The authors declare no conflict of interest.

References

1. C. W. Tang and S. A. VanSlyke, "Organic electroluminescent diodes," Appl. Phys. Lett. **51**(12), 913-915 (1987).
2. C. Adachi, M. A. Baldo, M. E. Thompson, and S. R. J. J. o. A. P. Forrest, "Nearly 100% internal phosphorescence efficiency in an organic light-emitting device," **90**(10), 5048-5051 (2001).
3. T. Yamasaki, K. Sumioka, and T. Tsutsui, "Organic light-emitting device with an ordered monolayer of silica microspheres as a scattering medium," Appl. Phys. Lett. **76**(10), 1243-1245 (2000).
4. Y. Qu, J. Kim, C. Coburn, and S. R. Forrest, "Efficient, nonintrusive outcoupling in organic light emitting devices using embedded microlens arrays," ACS photonics **5**(6), 2453-2458 (2018).
5. J.-G. Zhou, X.-C. Hua, Y.-K. Chen, Y.-Y. Ma, C.-C. Huang, Y.-D. Wang, and M.-K. Fung, "Nano-modified indium tin oxide incorporated with ideal microlens array for light extraction of OLED," J. Mater. Chem. C **7**(13), 3958-3964 (2019).
6. J. Yang, Q. Bao, Z. Xu, Y. Li, J. Tang, and S. J. A. P. L. Shen, "Light out-coupling enhancement of organic light-emitting devices with microlens array," Appl. Phys. Lett. **97**(22), 256 (2010).
7. S. Möller and S. Forrest, "Improved light out-coupling in organic light emitting diodes employing ordered microlens arrays," J. Appl. Phys. **91**(5), 3324-3327 (2002).
8. Y. Sun and S. R. Forrest, "Organic light emitting devices with enhanced outcoupling via microlenses fabricated by imprint lithography," J. Appl. Phys. **100**(7), 073106 (2006).
9. H.-W. Chang, J. Lee, S. Hofmann, Y. Hyun Kim, L. Müller-Meskamp, B. Lüssem, C.-C. Wu, K. Leo, and M. C. Gather, "Nano-particle based scattering layers for optical efficiency enhancement of organic light-emitting diodes and organic solar cells," J. Appl. Phys. **113**(20), 204502 (2013).
10. C. Lee and J. J. Kim, "Enhanced light out-coupling of OLEDs with low haze by inserting randomly dispersed nanopillar arrays formed by lateral phase separation of polymer blends," Small **9**(22), 3858-3863 (2013).
11. T.-W. Koh, J. A. Spechler, K. M. Lee, C. B. Arnold, and B. P. Rand, "Enhanced outcoupling in organic light-emitting diodes via a high-index contrast scattering layer," ACS photonics **2**(9), 1366-1372 (2015).
12. W. H. Koo, S. M. Jeong, F. Araoka, K. Ishikawa, S. Nishimura, T. Toyooka, and H. Takezoe, "Light extraction from organic light-emitting diodes enhanced by spontaneously formed buckles," Nat. Photonics **4**(4), 222-226 (2010).
13. J.-H. Jang, M.-C. Oh, T.-H. Yoon, and J. C. Kim, "Polymer grating imbedded organic light emitting diodes with improved out-coupling efficiency," Appl. Phys. Lett. **97**(12), 203 (2010).
14. H. Liang, H. C. Hsu, J. Wu, X. He, M. K. Wei, T. L. Chiu, C. F. Lin, J. H. Lee, and J. Wang, "Corrugated organic light-emitting diodes to effectively extract internal modes," Opt. Express **27**(8), A372-A384 (2019).
15. X. Fu, Y. A. Chen, D. H. Shin, Y. Mehta, I. T. Chen, N. Barange, L. Zhu, S. Amoah, C. H. Chang, and F. So, "Recovering cavity effects in corrugated organic light emitting diodes," Opt. Express **28**(21), 32214-32225 (2020).
16. Y. Sun and S. R. Forrest, "Enhanced light out-coupling of organic light-emitting devices using embedded low-index grids," Nat. Photonics **2**(8), 483-487 (2008).
17. T. W. Koh, J. M. Choi, S. Lee, and S. Yoo, "Optical outcoupling enhancement in organic light-emitting diodes: highly conductive polymer as a low-index layer on microstructured ITO electrodes," Adv. Mater. **22**(16), 1849-1853 (2010).
18. M. Slootsky and S. R. Forrest, "Enhancing waveguided light extraction in organic LEDs using an ultra-low-index grid," Opt. Lett. **35**(7), 1052-1054 (2010).
19. X.-L. Zhang, J. Feng, X.-C. Han, Y.-F. Liu, Q.-D. Chen, J.-F. Song, and H.-B. Sun, "Hybrid Tamm plasmon-polariton/microcavity modes for white top-emitting organic light-emitting devices," Optica **2**(6), 579-584 (2015).
20. P. Dyreklev, M. Berggren, O. Inganäs, M. R. Andersson, O. Wennerström, and T. Hjertberg, "Polarized electroluminescence from an oriented substituted polythiophene in a light emitting diode," Adv. Mater. **7**(1), 43-45 (1995).

21. M. Jandke, P. Strohriegl, J. Gmeiner, W. Brütting, and M. Schwoerer, "Polarized Electroluminescence from Rubbing-Aligned Poly (p-phenylenevinylene)," Adv. Mater. **11**(18), 1518-1521 (1999).
22. V. Cimrová, M. Remmers, D. Neher, and G. Wegner, "Polarized light emission from LEDs prepared by the Langmuir-Blodgett technique," Adv. Mater. **8**(2), 146-149 (1996).
23. D.-M. Lee, Y.-J. Lee, J.-H. Kim, and C.-J. Yu, "Birefringence-dependent linearly-polarized emission in a liquid crystalline organic light emitting polymer," Opt. Express **25**(4), 3737-3742 (2017).
24. D. Yokoyama, "Molecular orientation in small-molecule organic light-emitting diodes," J. Mater. Chem. **21**(48), 19187-19202 (2011).
25. T. Höfler, M. Weinberger, W. Kern, S. Rentenberger, and A. Pogantsch, "Modifying the Output Characteristics of an Organic Light-Emitting Device by Refractive-Index Modulation," Adv. Funct. Mater. **16**(18), 2369-2373 (2006).
26. G. Koch, "Liquid crystal photoalignment materials.," U.S. patent 9,508,942 B2 (Nov 29, 2016).
27. S. H. Kim, I. Cho, M. K. Sim, S. Park, and S. Y. Park, "Highly efficient deep-blue emitting organic light emitting diode based on the multifunctional fluorescent molecule comprising covalently bonded carbazole and anthracene moieties," J. Mater. Chem. **21**(25), 9139-9148 (2011).
28. D. Yokoyama, K. Nakayama, T. Otani, and J. Kido, "Wide-range refractive index control of organic semiconductor films toward advanced optical design of organic optoelectronic devices," Adv. Mater. **24**(47), 6368-6373 (2012).
29. M. Vuks, "Determination of the optical anisotropy of aromatic molecules from the double refraction of crystals," Opt. Spektrosk. **20**, 361 (1966).
30. M. K. Callens, D. Yokoyama, and K. Neyts, "Anisotropic materials in OLEDs for high outcoupling efficiency," Opt. Express **23**(16), 21128-21148 (2015).
31. A. Salehi, X. Fu, D. H. Shin, and F. So, "Recent Advances in OLED Optical Design," Adv. Funct. Mater. **29**(15), 1808803 (2019).
32. J. W. Kim, J. H. Jang, M. C. Oh, J. W. Shin, D. H. Cho, J. H. Moon, and J. I. Lee, "FDTD analysis of the light extraction efficiency of OLEDs with a random scattering layer," Opt. Express **22**(1), 498-507 (2014).
33. H. Cho, J. Chung, J. Song, J. Lee, H. Lee, J. Lee, J. Moon, S. Yoo, and N. S. Cho, "Importance of Purcell factor for optimizing structure of organic light-emitting diodes," Opt. Express **27**(8), 11057-11068 (2019).
34. L. Zhou, Y. F. Zhu, Q. Y. Zhang, Y. Zhou, Y. Z. Wang, G. H. Zhou, H. X. Wei, and S. Shen, "Highly linearly polarized light emission from flexible organic light-emitting devices capitalized on integrated ultrathin metal-dielectric nanograting," Opt. Express **28**(9), 13826-13836 (2020).
35. J. Frischeisen, Q. Niu, A. Abdellah, J. B. Kinzel, R. Gehlhaar, G. Scarpa, C. Adachi, P. Lugli, and W. Brütting, "Light extraction from surface plasmons and waveguide modes in an organic light-emitting layer by nanoimprinted gratings," Opt. Express **19**(101), A7-A19 (2011).
36. Y. Wang, J. Shi, J. Chen, W. Zhu, and E. Baranoff, "Recent progress in luminescent liquid crystal materials: design, properties and application for linearly polarised emission," J. Mater. Chem. C **3**(31), 7993-8005 (2015).
37. G. Koch and N. Copner, "Organic light emitting diode devices," U.S. patent 9,130,193 B2 (Sep 8, 2015).